Chapter 3

Dye Sensitized Solar Cells Based on ZnO Nanostructures and Organic Dyes

This Page is intentionally left blank

3.1. Introduction

With the increasing world population, spreading urbanization and technological advancement, matching the energy supply with the energy demand is the major challenging issue the world is facing these days. The environmental consequences related to extensive use of fossil fuels, safety related issues of nuclear power, ever-growing energy demand and depleting the stock of fossil fuels have motivated the researchers to search for alternative economically and environmentally sustainable renewable energy sources [1]. In such a context of global energy requirements, among all the non-polluting and renewable energy sources, the photovoltaic technology utilizing solar energy has emerged as the most assuring candidate [2]. Though conventional photovoltaic devices (silicon-based solar cells) are promising for the direct conversion of photons into electrons, the prohibitive cost of these cells is non-competitive with conventional power generating methods [3, 4]. On the contrary, dye-sensitized solar cells (DSSCs), invented by O'Regan and Grätzel in 1991, are non-conventional photovoltaic technology based solar cells that have attracted significant attention because of their novel fabrication concept derived from nature's principle (photosynthesis), easy fabrication procedure using abundant materials, cost-effectiveness, suitability for a wide variety of end-user products and can be made flexible. SSC is a device that performs the conversion solar energy into electrical energy based on the principle of sensitization of wide band-gap semiconductors [5]. The photoelectrochemical performance of a DSSC mainly depends on the selected Photoanode material, including its surface morphology and the sensitizing dye used [6-9]. Although a large number of different DSSCs have been investigated, most of them are not commercially popular until now because of their issues with low conversion efficiency, higher production cost, lower stability and durability [10, 11]

Different inorganic, organic and hybrid dyes were employed as sensitizers in DSSCs. But among all of them, the ruthenium complexes are the

most popular sensitizers because of But among all of them, the ruthenium complexes are the most popular sensitizers because of their exceptional charge transfer mechanics and absorption across the complete visible range along with intense metal-to-ligand charge transfer mechanism [12]. But the significant downsides of Ruthenium dyes are its rareness, high cost and complicated synthesis process [13].Also, ruthenium polypyridyl complexes contain heavy metal, which is harmful to the environment [14]. In order to find out low-cost and environment-friendly alternatives to these expensive ruthenium compounds, researchers are focusing on easily available natural dyes extracted from various natural resources. Many researchers have studied sensitizing effects of several natural dyes derived from various fruits, flowers and leaves [15]. Most of them are used with TiO_2 nanostructures as photoanode[16-20]. However, ZnO has recently emerged as a great potential alternative to TiO2 due to its fascinating electrical and optical properties. ZnO is a wide band gap semiconductor having a direct band gap of 3.37 eV, making it suitable as a photoanode material for DSSC [21, 22]. Apart from this, ZnO is very easy to synthesis, abundant, inexpensive and poses higher electron mobility (200-300 $cm^2V^{-1}S^{-1}$for bulk material and 1000 $cm^2V^{-1}S^{-1}$ for nanowire) than that of TiO_2 nanoparticles (0.1-4$cm^2V^{-1}S^{-1}$) [23-25]. Moreover, the 1-D single-crystalline rod-like structure of ZnO nanorods provides a higher surface-to-volume ratio enabling better dye loading [26]. These qualities of ZnO make it a potential alternative to TiO_2 for the fabrication of DSSCs.

In this study, we aimed to combine natural sensitizers with two types of nanostructured ZnO to get both the advantages of ZnO and also the benefits of natural organic dyes targeting lower fabrication cost, echo-friendly devices along with good cell performance and wanted to find out the best suitable ZnO nanostructure-Natural dye combination. In this regard, we fabricated four DSSCs using two types of natural dyes, anthocyanin extracted from pomegranate (*Punica granatum*) and curcumin extracted from fresh

turmeric(*Curcuma longa*) and their electro-optical responses to investigate their usefulness as natural sensitizers when adsorbed onto ZnO nanorod (NR) and ZnO nanoparticle (NP) films in DSSCs has been studied. Hydroxyl and Carbonyl groups existing the natural sensitizers bound them easily to the surface of the ZnO nanorods, which facilitates very easy electron injection from LUMO of dye molecule to the conduction band of ZnO [27]. Along with that, we have also studied the effect of Rose Bengal as sensitizing dye in TiO_2 and ZnO nanoparticle based DSSCs.

3.2. Experimental Section

3.2.1. *Structure and Working principle of DSSC*

A typical DSSC consists of four elements: a photoanode with a thin layer of mesoporous wide bandgap semiconductor oxide layer (usually TiO_2, ZnO, SnO_2 or Nb_2O_5)over a transparent conducting substrate (ITO or FTO), a monolayer of the sensitizing dye adsorbed on the semiconductor oxide surface to facilitate light absorption, a redox mediator electrolyte solution (typically I^- / I_3^-) in an organic solvent and a counter electrode made up of a catalyst (platinized ITO or FTO) to facilitate charge collection. The schematic of device architecture and working principle of a typical DSSC is shown in Fig. 3.1(a) and Fig. 3.1(b). Upon exposure to the sunlight, dye molecule absorbs photon energy and goes through an electronic state change, the electron jumps from ground state (HOMO) to the excited state (LUMO). As a result, electron injection into the conduction band of the semiconductor oxide (ZnO) film occurs, whereby the dye molecule gets oxidized. This oxidized dye molecule is regenerated by taking an electron from the redox species of the electrolyte (I^-).Subsequently, I^- is regenerated by reduction of I_3^- with electrons migrated from photo anode via external load and collected at the counter electrode, completing the cycle [5, 6].

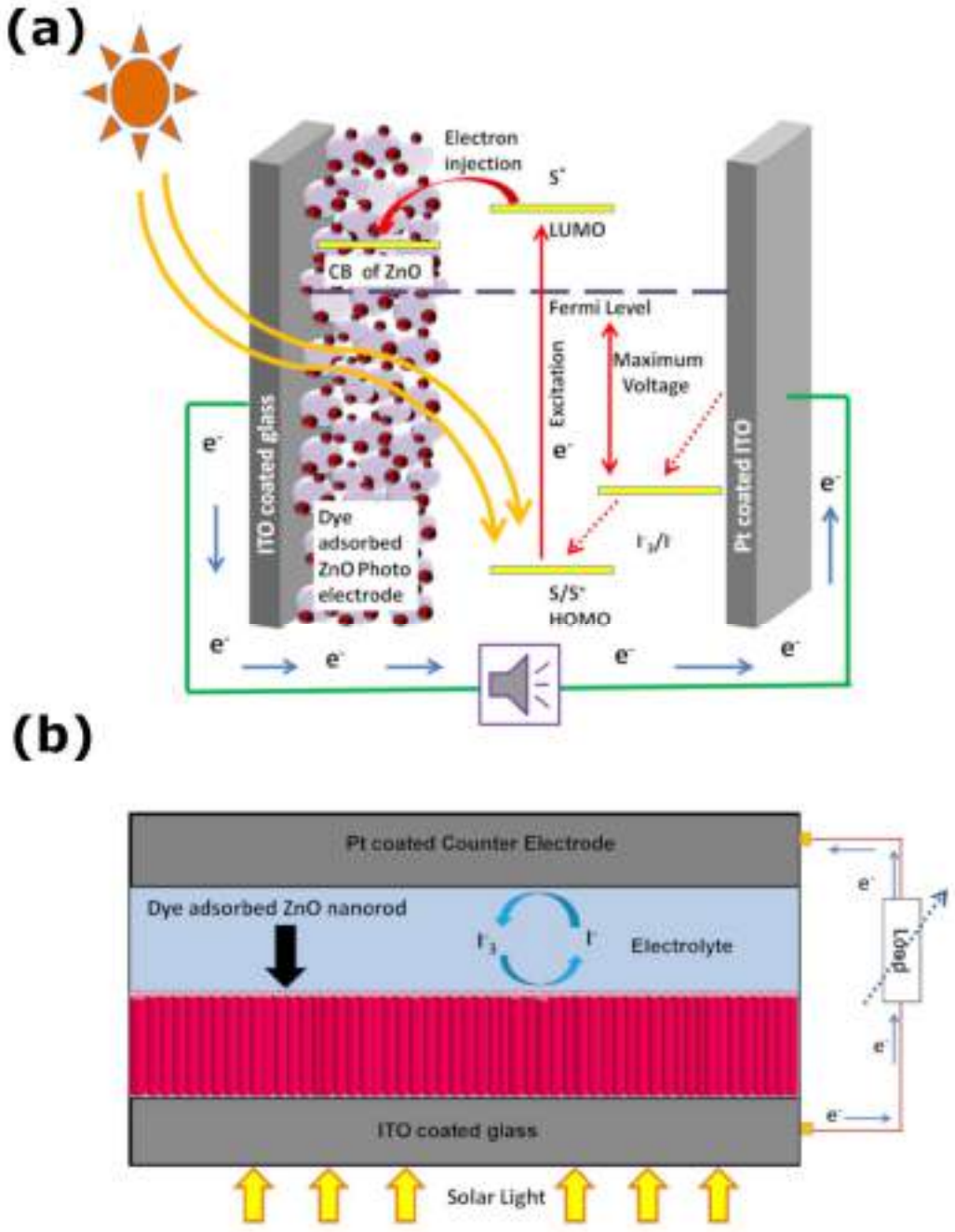

Figure 3.1 Schematic diagram and basic working mechanism of DSSCs based on (a) ZnO nanoparticle (b) ZnO nanorod.

3.2.2. *Materials used*

Transparent ITO coated glass (10 Ω/ square) was purchased from Techinstro, India. The liquid platinum paint (Platisol T) purchased from Solaronix, Switzerland, was used to prepare the platinum-coated transparent counter electrode. Commercial ZnO and TiO_2 nanopowder , Zinc acetate dehydrate, Hexamethylenetetramine and Rose Bengal dye, all were purchased from Sigma Aldrich. Ethylene Glycol (Sigma Aldrich) was used as a solvent for the electrolyte preparation using KI (S D Fine-Chemical Ltd., India) and I_2 (RANKEM, India). Meltonix 1170-60(60μm) purchased from Solaronix was used as a spacer between the electrodes to avoid short-circuiting between the ITO and electrolyte.

3.2.3. *Extraction and Preparation of Organic Dye Sensitizers*

In the fabrication of Dye Sensitized solar cells, selecting the dyes is a crucial task as it significantly affects the performance and production cost of the cells. By choosing abundant natural dyes instead of expensive synthetic ruthenium dyes we can reduce the production cost by a large amount. In this work, we have chosen Curcumin and pomegranate juice extracts as sensitizers. Curcumin was extracted by grinding turmeric root in an iron mortar and then mixing in 100ml ethanol. After extraction, Solid residues were filtered out to obtain a clear natural dye solution.

For pomegranate extraction of pomegranate juice, afresh pomegranate was squeezed and mixed with 100ml deionized water. This solution is also filtered to obtain pure dye. The dye solutions were properly stored, protecting from direct sunlight for further use. Studies have shown that Curcumin dyes have two forms and they are identified as Keto and Enol [28]. On the contrary, it was found that pomegranate juice mostly contains six types of anthocyanins. These are cyanidin 3-glucoside, cyanidin 3,5-diglucoside, delphinidin 3-glucoside, delphinidin 3,5-diglucoside, pelargonidin 3-glucoside and

pelargonidin 3,5-diglucoside [29]. The chemical structures of these dyes are shown in Fig. 3.2.

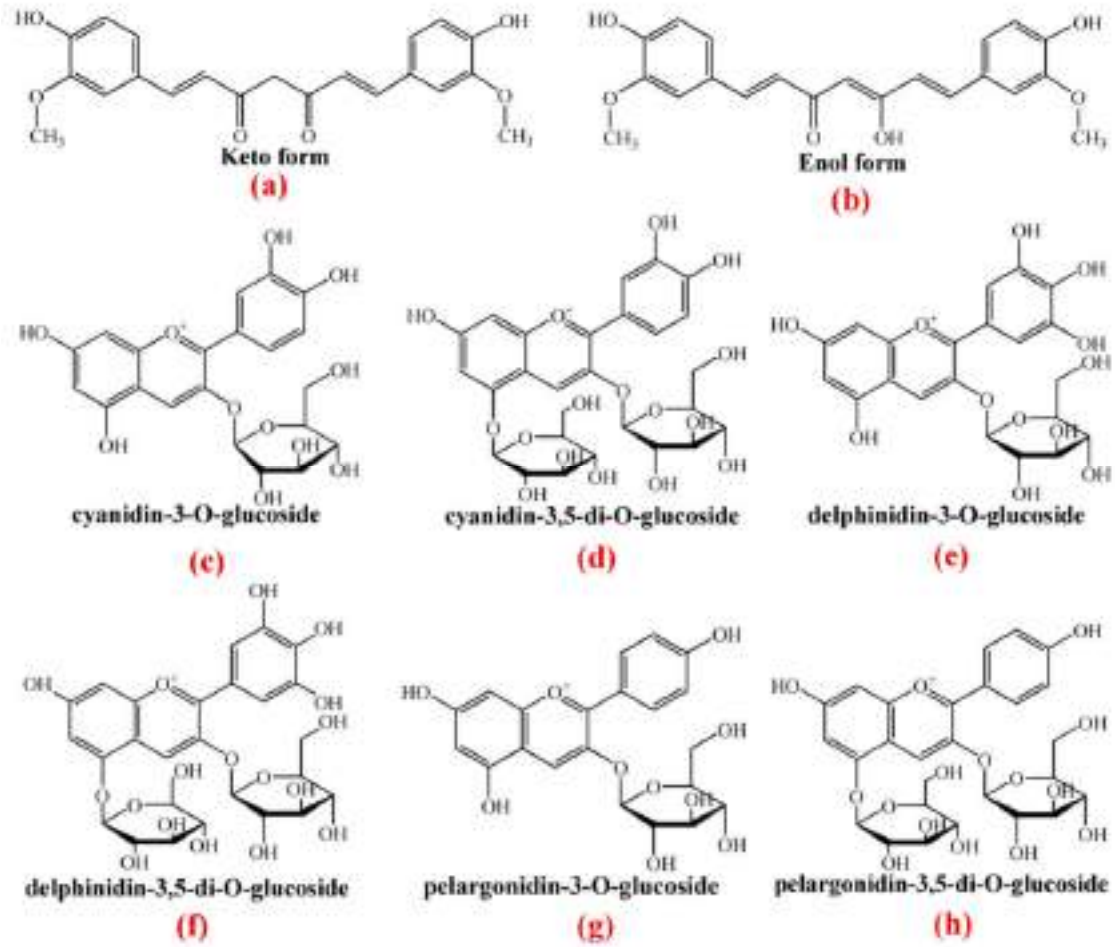

Figure 3.2 Chemical structures of Curcumin (a & b) present in turmeric and six major anthocyanins (c- h) present in Pomegranate fruit extracts.

For Rose Bengal dye sensitization, 0.5 mM ethanolic solution of pure Rose Bengal dye was prepared. Chemical structure of rose bengal dye is shown Fig. 3.3.

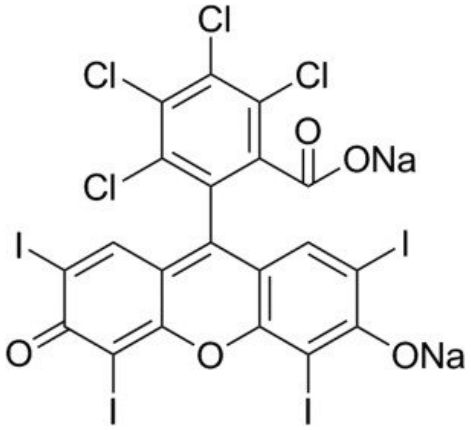

Figure 3.3 Chemical structure of Rose Bengal dye.

3.2.4. *Preparation of working electrodes*

To prepare the working electrode, first, the ITO coated glass was cut into 2×2cm square shaped pieces. Cleaning of this substrate is very important as it removes any organic or inorganic contaminant present on its surface which can significantly affect the performance of the cells. Furthermore, cleaning enhances the adhesion of the subsequent layers to be deposited over it. The ITO substrates were cleaned using dilute HCl for 15 minutes in an ultrasonic cleaner to remove oxide impurities. Then they were rinsed extensively with deionized water to remove the HCl residues. The substrates were then cleaned in acetone, ethanol and deionized water for 15 minutes each using an ultrasonic bath. Finally, the substrates were dried using a hairdryer. The cleaned substrates were masked using scotch tape on four sides, leaving the central area empty for semiconductor material deposition.

ZnO nanorods were grown on the ITO coated glass substrate following a simple two-step Sol-Gel spin coating protocol followed by hydrothermal growth [30]. In the first step, a thin ZnO seed layer was formed on the ITO glass substrates using 5mMZinc acetate dehydrate $(CH_3COO)_2Zn$, $2H_2O$, (98% Merck) in acetone as precursor solution. The solution was mixed well using an ultrasonic bath for 2 hours at room temperature and spun onto cleaned and masked ITO coated glass substrates using a programmable spin coater (Apex Technologies, Model SCU-2008C) at 1000 rpm for 30 seconds. The coated

substrates were then annealed at 350^{o}Ctemperature for 30 minutes. After evaporation of the solvent, a thin ZnO film was formed whose thickness can be controlled by repeating the above process. In this way, the seed layer is formed. The thickness of the film can also be controlled by varying solution concentrations and the spinning speed of the spin coater [31]. In the second step, vertically aligned ZnO nanorods were grown over the seed layer coated ITO glass substrate by hydrothermal method. In this method, the seed layer coated substrate was immersed in a solution containing an equal proportion of 5mM Zinc acetate dehydrate $(CH_3COO)_2Zn$, $2H_2O$ and 5mM Hexamethylenetetramine ($C_6H_{12}N_4$) at 90^{o}C temperature in a Pyrex vessel for 2 hours. This creates an array of vertically aligned ZnO nanorods on the substrate. It was then taken out from the solution and rinsed immediately with ethanol and deionized water to remove any leftover residues from the film surface and allowed to air dry at room temperature. Finally, the ZnO nanorod formation was completed by annealing the film at 450^{o}C for 30min. This ZnO nanorod array coated substrates were then immersed in the dye solutions to allow adsorption of the dye molecules onto the semiconductor nanorod surface for 24 hours. Then the electrodes were taken out from the solutions and rinsed with ethanol and deionized water to remove the excess dye from the photoanode surface of the films and air-dried at room temperature. The counter electrode was prepared by spin coating the platinum precursor solution (platisol T–solaronix) at 1000 rpm for 30 seconds onto a drilled ITO substrate and giving heat treatment at 450^{o}C for 15 minutes. The flow chart representing the whole process of growth of the ZnO nanorods is shown in Fig. 3.4. below.

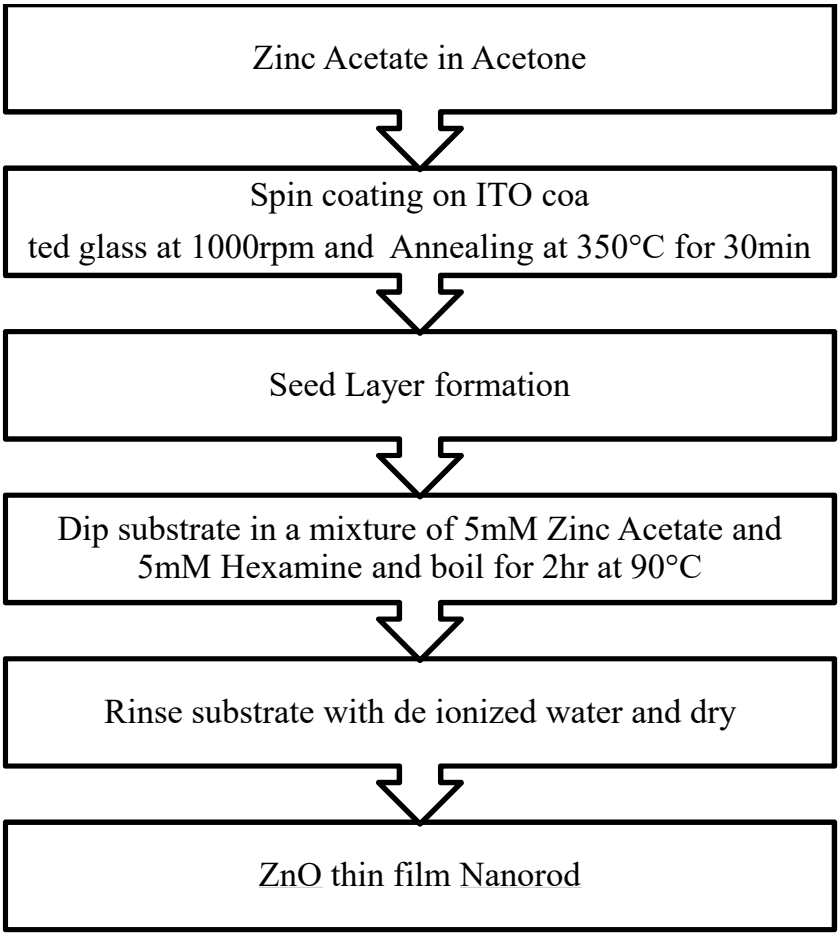

Figure 3.4 Flow chart for preparation of ZnO nanorod layer.

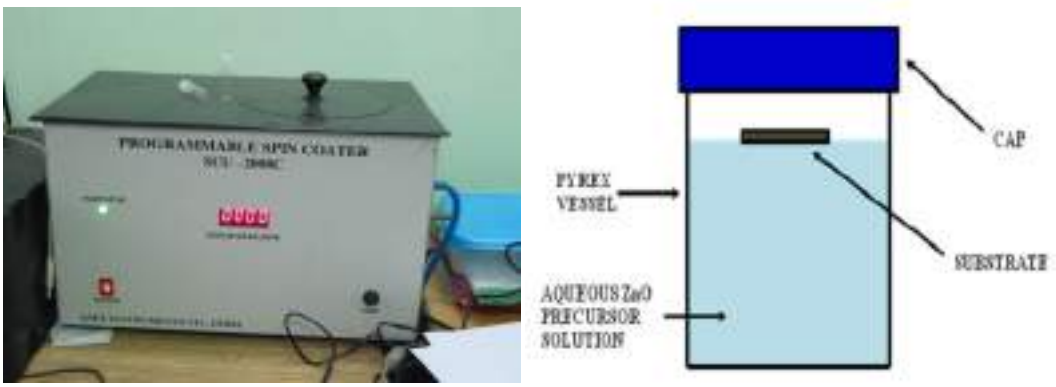

Figure 3.5 (a) Spin Coater for seed layer formation (b) vessel for nanorod grow.

On the other hand, the nanopowder based photoelctrodes were prepared by doctor blade method. At first, 10 gm of the nanopowder was mixed with diluted acetic (1ml in 50 ml deionized water) acid in a mortar and pastel and

added a few drops of Triton X100 (Merck) as surfactant and ground continuously until a homogenous, smooth suspension was obtained. The lump-free slurry was then applied on the conductive side of an ITO-coated glass using the doctor blade method to make a homogeneous layer. To strengthen the bonding between the ITO glass and the semiconductor paste, the nanopowder coated ITO glass plates were sintered in normal atmospheric condition at 450°C for 45 minutes. In the sintering process, after introducing the sample in the furnace, the temperature was raised with a rate of 10°C/5 min until the temperature had reached 350°C and after that, it was increased with a rate of 10°C/10 min until 450°C. When it cooled down to room temperature, the sintered substrates were immersed in the Rose Bengal dye solution for dye adsorption on the surface of the TiO_2 and ZnO nanoparticles for 24 hours. Image of TiO_2 photoanode during sintering process and after sintering is shown in Fig. 3.6.

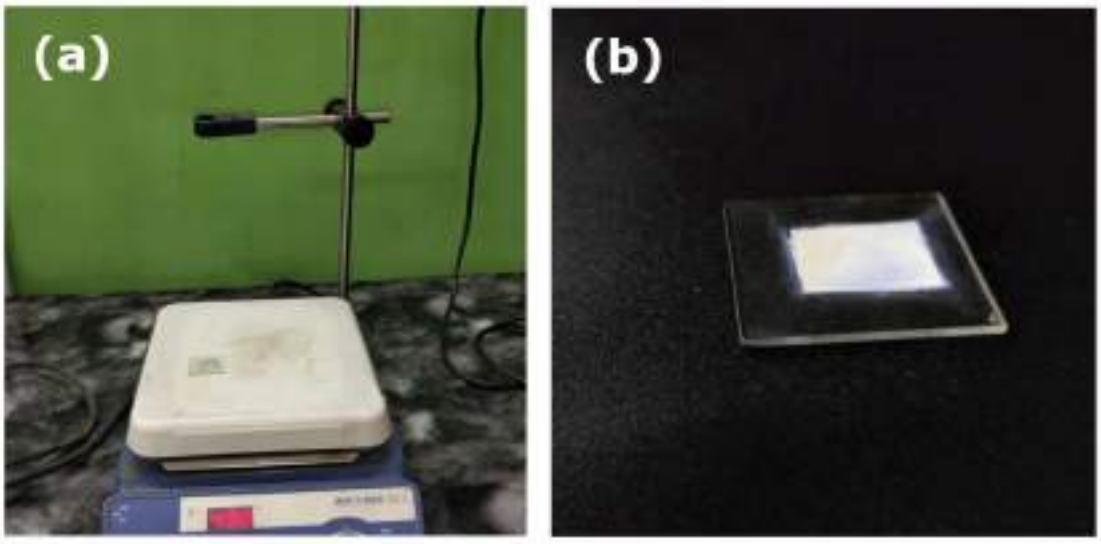

Figure 3.6 TiO_2 nanopowder coated ITO (a) during sintering process (b) after sintering.

3.2.5. *DSSC assembling*

To assemble the solar cell, the conductive side of the platinum coated counter electrode was placed over the dye adsorbed ZnO nanorod photoanode

so that the platinized side of the counter electrode faces the ZnO film. Surlyn spacer (Meltonix 1170-25µm) was placed between them to prevent the uncoated areas of the electrodes from short-circuiting. Two binder clips were used to firmly clamp the two electrodes together in a sandwich manner. The redox electrolyte was prepared by mixing 0.5 M KI and 0.05 M I_2 in Ethylene Glycol (Fig. 3.7 (b)) solvent in a proportionate amount. This electrolyte solution was injected into the cell through the drilled hole on the counter electrode. The hole was then sealed using a hot melt sealant. The effective cell area was 1 cm^2. Fig. 3.7(a) depicts the picture of a complete cell fabricated using ZnO nanoparticle and curcumin dye.

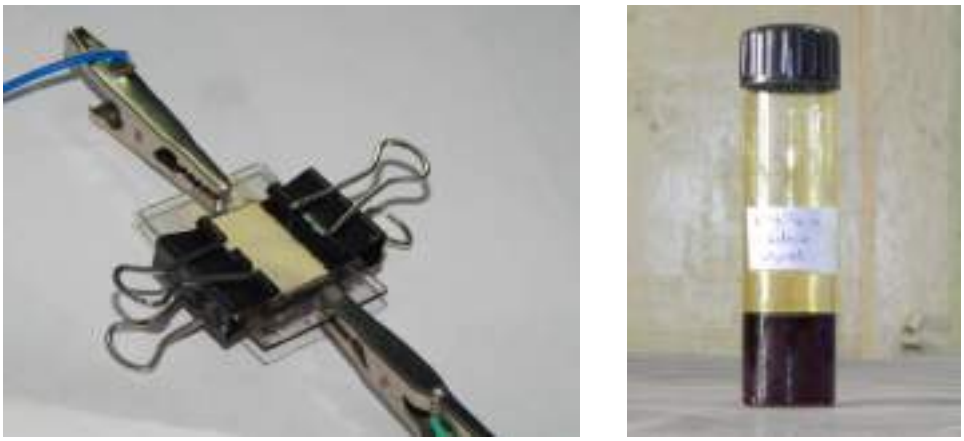

Figure 3.7 (a) Cell Fabricated with Curcumin dye (b) KI + I_2 Electrolyte.

3.2.6. *Device Characterization and Measurements*

The absorption spectra of the dyes were studied using a Perkin Elmer Lambda–35 UV-VIS spectrophotometer in the wavelength range of 200-600nm range. The crystalline structure of the ZnO films was studied using a PANalytical X'Pert PRO X-ray diffractometer with CuKα (30mA, 40 kV, λ= 1.5406 Å). The surface morphologies of the ZnO films were characterized by using scanning electron microscopy (JEOL). The current-voltage (I-V) characteristics of the fabricated cells under illumination of 100mW/cm^2 (Oriel Xenon lamp 450W) were recorded by employing a Keithley 2400 source meter connected to a PC.

3.3. Results and Discussion

3.3.1. *UV-VIS absorption spectral analysis of the dyes*

UV-VIS absorption spectra of the Curcumin, pomegranate and Rose Bengal dye are shown in Fig. 3.8. A clear difference among the absorption peaks of the dyes can be seen. Curcumin exhibits an absorption peak at 422 nm, whereas pomegranate fruit extract solution at 517 nm. The Rose Bengal shows absorption peak at 549 nm. The difference in the absorption peaks is due to the different types of colours and chromophores present in curcumin, pomegranate and Rose Bengal dyes.

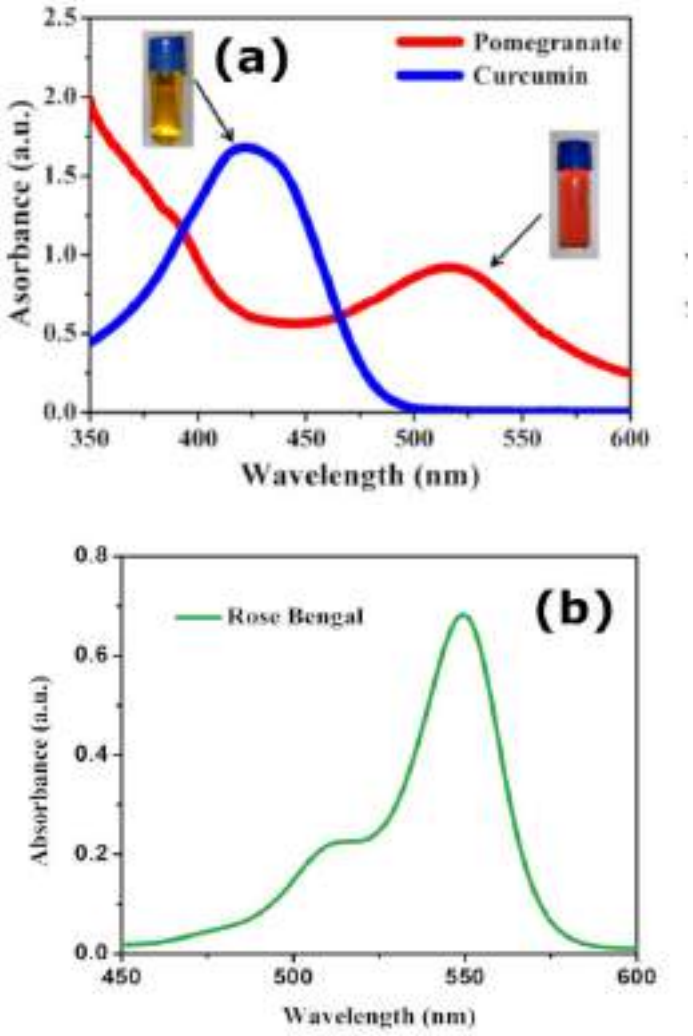

Figure 3.8 Absorption spectra of the (a) curcumin and anthocyanin (pomegranate) (b) Rose Bengal sensitizers used to fabricate DSSCs.

3.3.2. *X-ray diffraction analysis of the ZnO film*

The structural and crystalline quality information of the synthesized ZnO nanorods, purchased ZnO and TiO_2 nanoparticles were studied using X-Ray diffraction pattern of the samples and shown in Fig. 3.9, Fig. 3.10 and Fig. 3.11 respectively. The consistency of the obtained diffraction peaks of ZnO samples were confirmed by comparing them with the standard JCPS card no. 36-1451. A remarkably enhanced diffraction peak for the (002) plane at 34.4595 ^{o} can be clearly observed for the ZnO Nanorods. It indicates strong preferential growth of ZnO nanorods along the c-axis and vertical alignment on the ITO substrate and the hexagonal wurtzite structure. XRD of TiO_2 and ZnO nanoparticles are shown in Fig. 3.10 and Fig. 3.11 respectively.

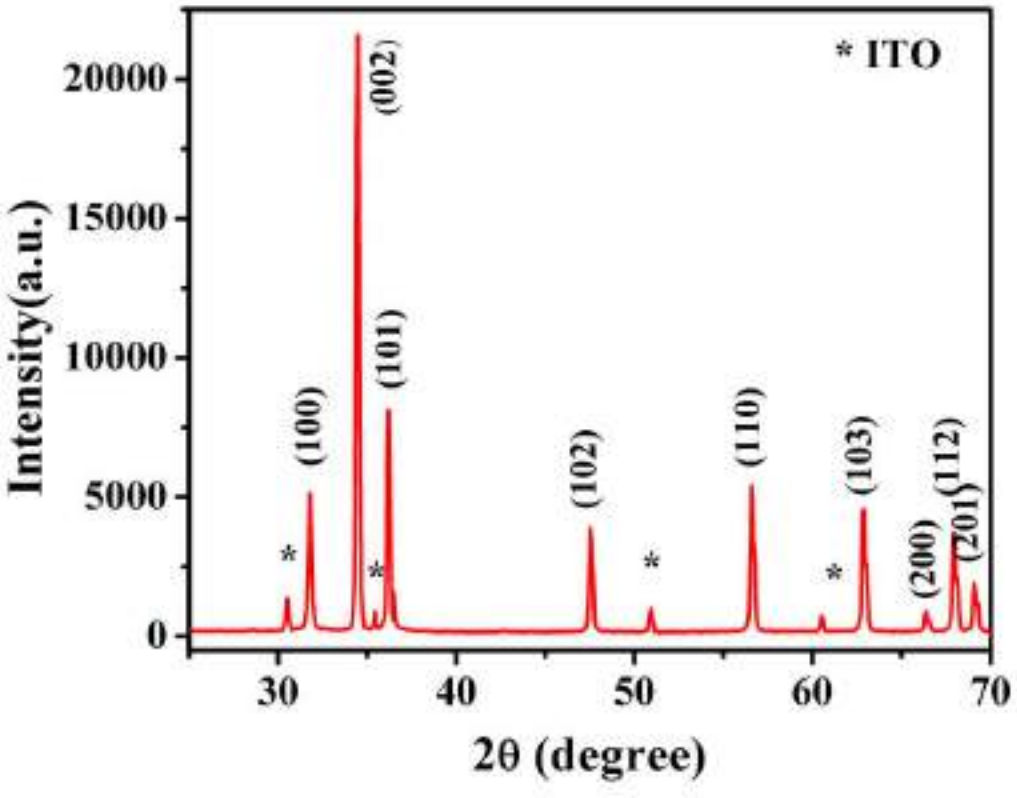

Figure 3.9 XRD pattern of the ZnO nanorods synthesized by a sol-gel spin coating method.

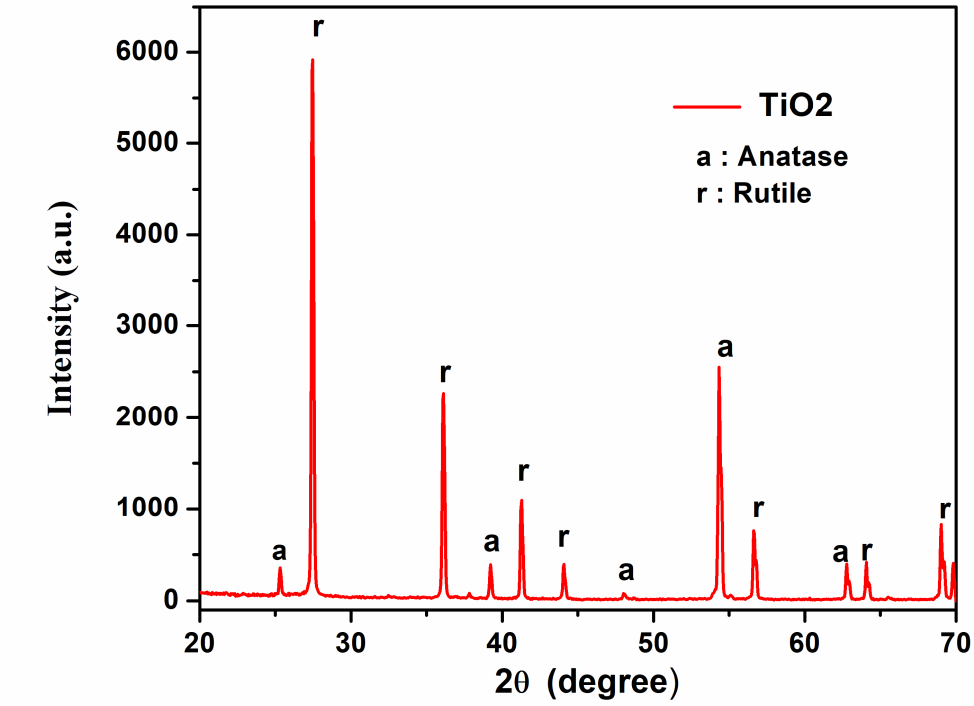

Figure 3.10 XRD of TiO_2 nanopowder.

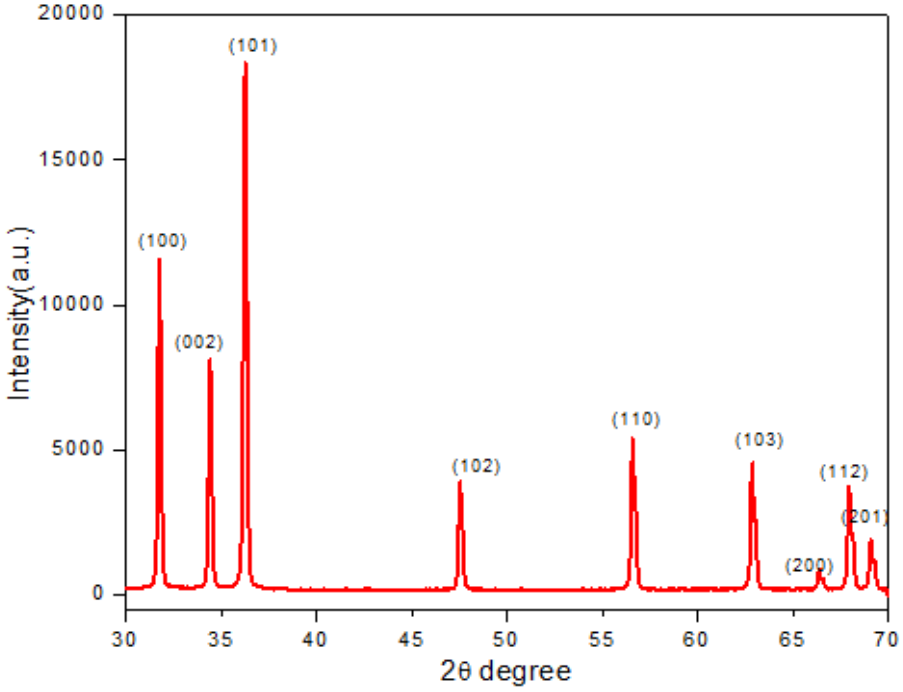

Figure 3.11 XRD of ZnO nanopowder

3.3.3. *Scanning Electron Microscope Studies*

Scanning electron microscopy (SEM) was carried out to study the morphological properties of the sample film. Fig. 3.12(a) shows the SEM image of the ZnO nanorod arrays on ITO substrate. The SEM observation reveals that most nanorods have grown vertical to the seed layer on the ITO substrate and have a hexagonal wurtzite structure. The nanorods have diameters ranging from 100-200 nm with an average length of 300 to 400 nm and in the case of nanoparticles, the average particle size was around 50nm. EDS analysis was performed to investigate the chemical composition of the nanorods, which is shown in Fig. 3.11(b). It clearly confirms the presence of Zn and O in the photoanode. The unidentified peaks are due to the presence of indium (In) and tin (Sn) in the ITO substrate. The SEM and EDS of TiO_2 nanopartilces are shown in Fig. 3.13.

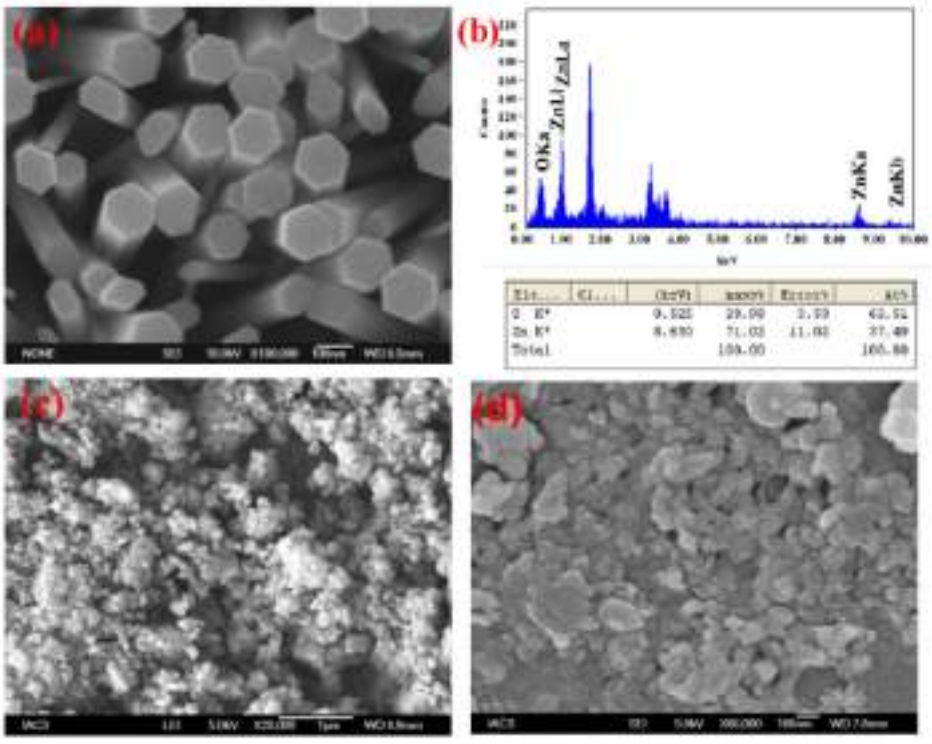

Figure 3.12 SEM image of (a) ZnO nanorods grown on ITO substrate (b) EDS spectra of the nanorod sample showing elemental composition (c) & (d) ZnO nanoparticle deposited sample at lower and higher magnification respectively.

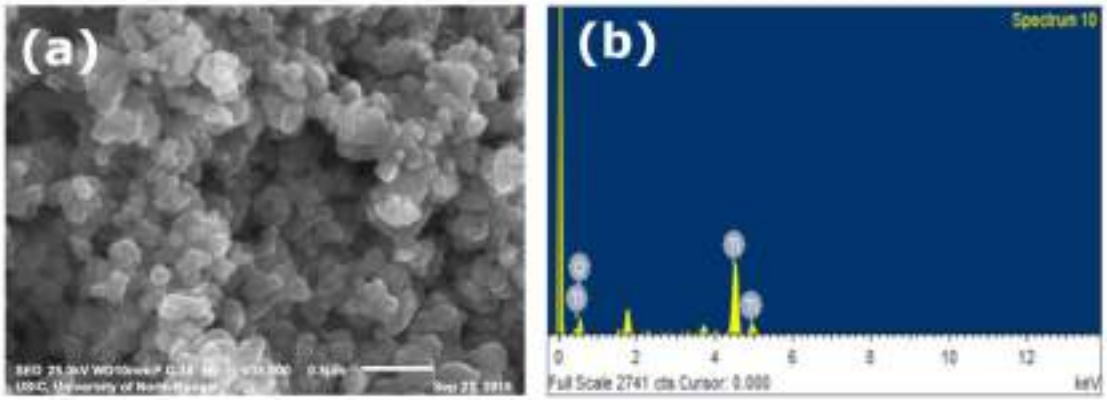

Figure 3.13 (a) SEM image of TiO_2 nanoparticles (b) EDS of TiO_2.

3.3.4. *Current-Voltage Characteristics study of the cells: Solar cell efficiency measurements*

The current-voltage characteristic of a Solar cell allows us to determine the photovoltaic performance of the cell. The J-V curves of the fabricated cells under the illumination of 100 mW/cm^2 are shown in Fig. 3.14 (a). The Power-Voltage plot to calculate the maximum power point (P_{max}), I_{max} and V_{max} are represented in Fig.3.14 (b). Table 3.1 shows various parameters extracted from the I-V curves of the ZnO nanorod-based DSSCs fabricated using natural dyes Curcumin and Pomegranate. The solar cell fabricated using Curcumin extract exhibits higher short-circuit photocurrent density (J_{SC}), open-circuit voltage (V_{OC}) and fill factor (FF) compared to the DSSC fabricated using pomegranate extract as a dye. In addition, the Curcumin dye cell shows an improved overall photoelectric conversion efficiency (η) over the anthocyanin dye cell. The efficiency of these natural dye-based cells may be low compared to the synthetic dye-based DSSCs, but these values are comparable to the efficiencies obtained for natural dye-based DSSCs reported by other researchers [33].

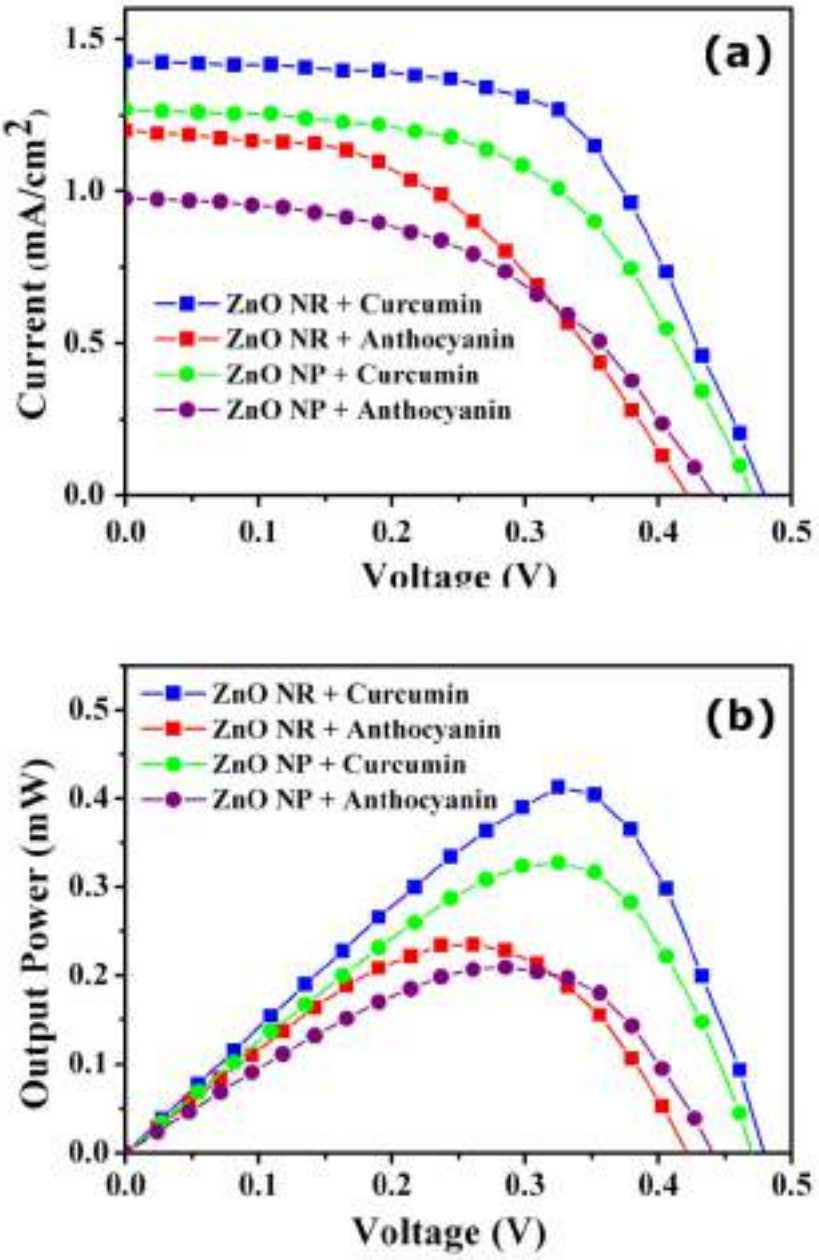

Figure 3.14 (a) Current density-Voltage characteristics of the natural dye based cells under illumination (b) Power-Voltage curve to obtain maximum power point.

Equivalent circuit modeling is a very important tool required for better understanding and explaining the solar cell performance and analysis of the electrical processes occurring inside the cell. The functioning of a solar cell is generally modeled by a single diode with a constantphoto-generated current

source, a series (R_s) and shunt resistance (R_{sh}) as shown in Fig.3.15. The current-voltage relation is given by the equation

$$I = I_{ph} - I_o \left[exp \left\{ \frac{(q(V + IR_s)}{Ak_BT} \right\} - 1 \right] - \frac{V + IR_s}{R_{sh}} \quad (1)$$

where I_{ph}, I_o,R_s,R_{sh}, q,A,k_B and T are the photocurrent, the saturation current of the diode, the series resistance, the shunt resistance, the electron charge, the ideality factor, the Boltzmann constant, and absolute temperature, respectively [34].

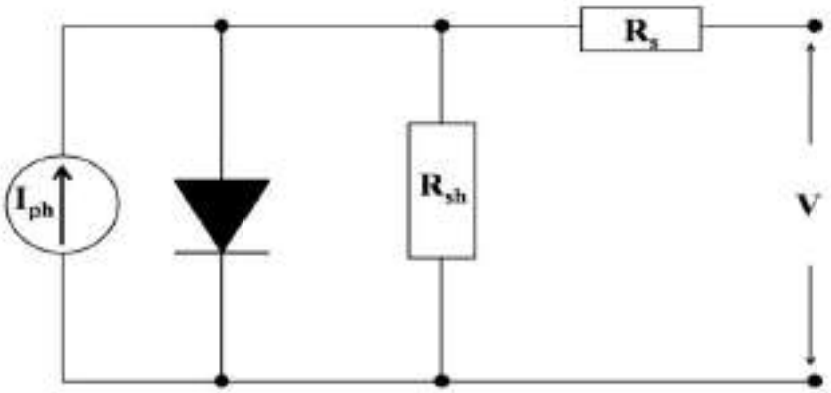

Figure 3.15 The equivalent circuit (single diode model) of a solar cell.

The circuit parameters like R_s and R_{sh} are not directly measurable. Instead, they are calculated by fitting the experimental J-V curve with the equation 1. Values of these parameters obtained for the fabricated cells are also represented in table 3.1.

Table 3.1. Solar Cell parameters of DSSC's fabricated with natural dyes.

Cell Name	Dye used & ZnO nanostructure	J_{sc} (mA/cm^2)	V_{oc} (V)	R_s (Ω cm^2)	R_{sh} (Ω cm^2)	FF	Efficiency (η %)
Cell-1	Curcumin & ZnO NR	1.43	0.49	86.28	7866.28	0.59	0.41
Cell-2	Anthocyanin & ZnO NR	1.20	0.43	116.67	2722.90	0.46	0.24
Cell-3	Curcumin & ZnO NP	1.27	0.46	101.19	6629.31	0.56	0.33
Cell-4	Anthocyanin & ZnO NP	0.98	0.45	146.87	4659.92	0.48	0.21

Cell-1 shows the lowest series resistance (R_s) compared to other cells. This indicates improved electrical contacts, lower junction resistances and better ZnO nanorod morphology in the case of cell-1. Higher series resistance means greater voltage drop inside the cell resulting in lower terminal voltage and sagging of current controlled part of the J-V curve towards the origin, which can be correlated with table 3.1 and Fig. 3.14(a). In addition, from the single diode equivalent circuit of the solar cell (Fig.3.15), it can be clearly seen that R_{sh} provides an alternative path to the photocurrent, which causes power losses in the solar cell. Lower R_{sh} results in partial shorting between the two electrodes of the solar cell giving rise to leakage current. So, the highest value of R_{sh} of cell-1 attributes to the lowest leakage current resulting in improved cell performance. Also, from table 3.1 it can be confirmed that higher shunt resistance results in a higher fill factor and consequently better photoconversion efficiency.

For DSSCs fabricated with Rose Bengal dye, In dark current measurement (Fig. 3.16 (a)) it was observed that TiO_2 cells shows higher dark current than ZnO cells, both sensitized with Rose Bengal dye. The dark current which actually flows in opposite direction to the original current minimizes the cell efficiency. Higher dark current of TiO_2 cell attributes to the lower efficiency.

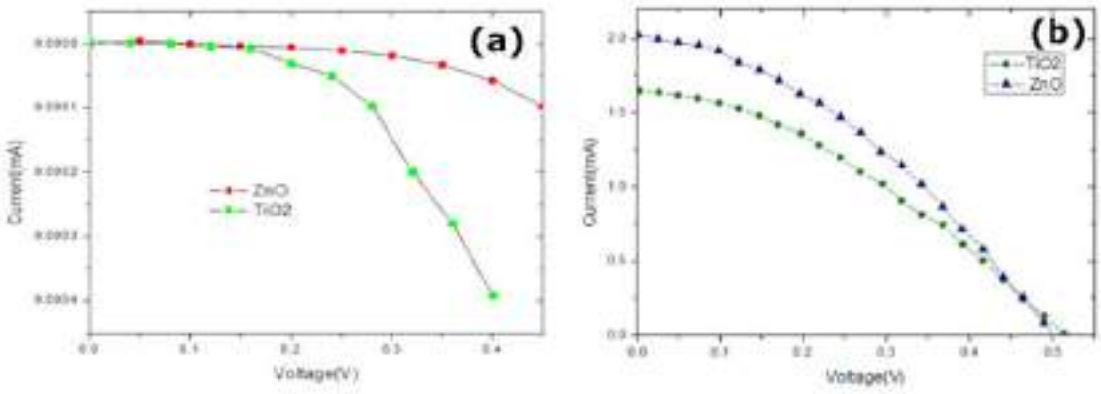

Figure 3.16 (a) Dark current measurement (b) I-V characteristics of the cells under illumination fabricated using TiO2 and ZnO.

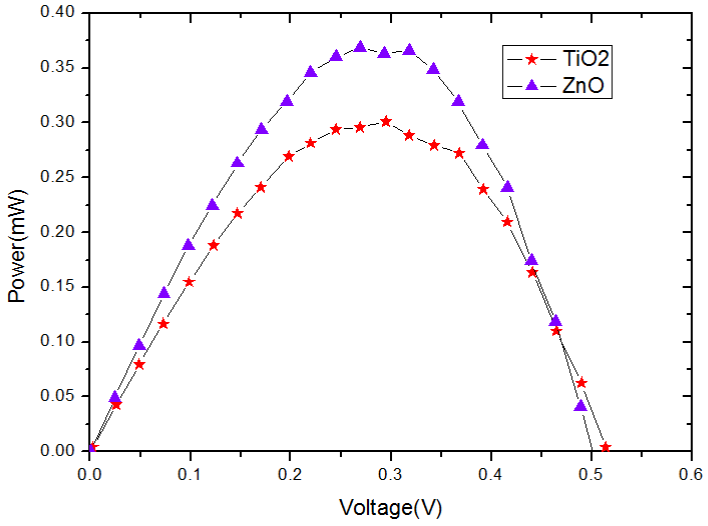

Figure 3.17 Power vs. Voltage graph of the cells fabricated with Rose Bnegal.

The I-V characteristic of the cells under illumination is shown in Fig. 3.16 (b). Fig. 3.17 displays the Power-Voltage curve to obtain maximum power points. Table shows comparative performance of the TiO_2 and ZnO cells in terms of open circuit voltage (V_{OC}), Short circuit current (I_{SC}), Fill Factor (FF) and energy conversion efficiency.

Table 3.2 Photovoltaic performance of the Rose Bengal sensitized cells.

Material	I_{SC} (mA/cm^2)	V_{OC}(V)	FF	Efficiency (η %)
TiO_2	1.65	0.514	0.35	1.18
ZnO	2.03	0.501	0.36	1.47

From table 3.2 we can see that ZnO cells are more efficient than TiO_2 cells when sensitized with Rose Bengal dye. This may be due better adsorption of Rose Bengal dye on ZnO nanoparticle surface than TiO_2 nanoparticle surface. Also the higher dark current of TiO_2 cell (shown in Fig.3.16(a)), which indicates higher recombination of electrons in case of TiO_2 cells than ZnO cells, attributing lower efficiency.

3.3.5. *Electrochemical impedance spectroscopy study of the cells*

The electrochemical impedance spectroscopy is a very useful diagnostic technique that has often been performed to investigate the interfacial charge transfer dynamics and recombination mechanisms occurring inside a DSSC [35]. These are generally modelled using the appropriate equivalent circuit in terms of resistors and capacitors. The EIS measurements were performed using HIOKI Impedance Analyser in the frequency range 0.1 Hz to 190 kHz under dark condition with employing an AC sinusoidal signal having an amplitude of 10mV under the influence of V_{oc} bias voltage. EIS findings as Nyquist plot of the DSSCs are shown in Fig. 3.18(a). Physical interpretation of the different electrochemical operations across the interfacial regions of the DSSCs can be done by fitting the EIS spectra with the equivalent circuit shown in Fig. 3.18(b).Generally a typical Nyquist plot exhibits three semicircles. However, only two semicircles are present in our study due to low-frequency limitation of our instrument. The first smaller semicircle (in the high-frequency range) attributes to the charge transfer resistance at the Pt counter electrode/Electrolyte interface (R_{CE}) and the second semicircle (mid-frequency range) having a higher diameter corresponds to the resistance of charge transfer and recombination process at the ZnO photoelectrode/dye/electrolyte interface (R_{ct}). The intercept of the first semicircle in the high-frequency range on the real axis of the Nyquist plot is associated with the contact resistances and external ohmic series resistance (R_{SER}) of the assembled cell [36]. The experimental Nyquist plot is fitted with the equivalent circuit shown in the inset of Fig. 3.18(a) using MEISP software by Kumho Chemical Laboratories, based on the algorithm developed by Prof. J. R. Macdonald (LEVM v7.0) for non-linear complex least square fitting, and the obtained parameters are represented in table 3.3. The chemical capacitance (C_{μ}) is very useful in illustrating the underlying mechanism through which photoelectrons store free energy and generates current and voltage in the outer circuit [37]. Also, the chemical

capacitance (C_μ) reflects charge carrier accumulation on the ZnO film and the density of states in the band-gap region [38]. From table 3.3, it can be seen that Cell-1 exhibits a much higher C_μ value than the other cells, which indicates the conversion of a higher amount of photon energy into chemical energy resulting in a higher amount of energy storage by virtue of carrier injection into the conduction band of ZnO. Reduced C_μ values for cell-2,3 &4 also suggest poor dye loading [39, 40]. It can also be observed from the Nyquist plot that the recombination resistance (R_{rec}) at the ZnO NR- Dye/ Electrolyte interface is highest for cell-1 compared to the other three cells. This shows that cell-1 has better resistance to the charge recombination between the photo-generated electrons and the electron acceptors in the red-ox electrolyte attributing lower recombination current [41].

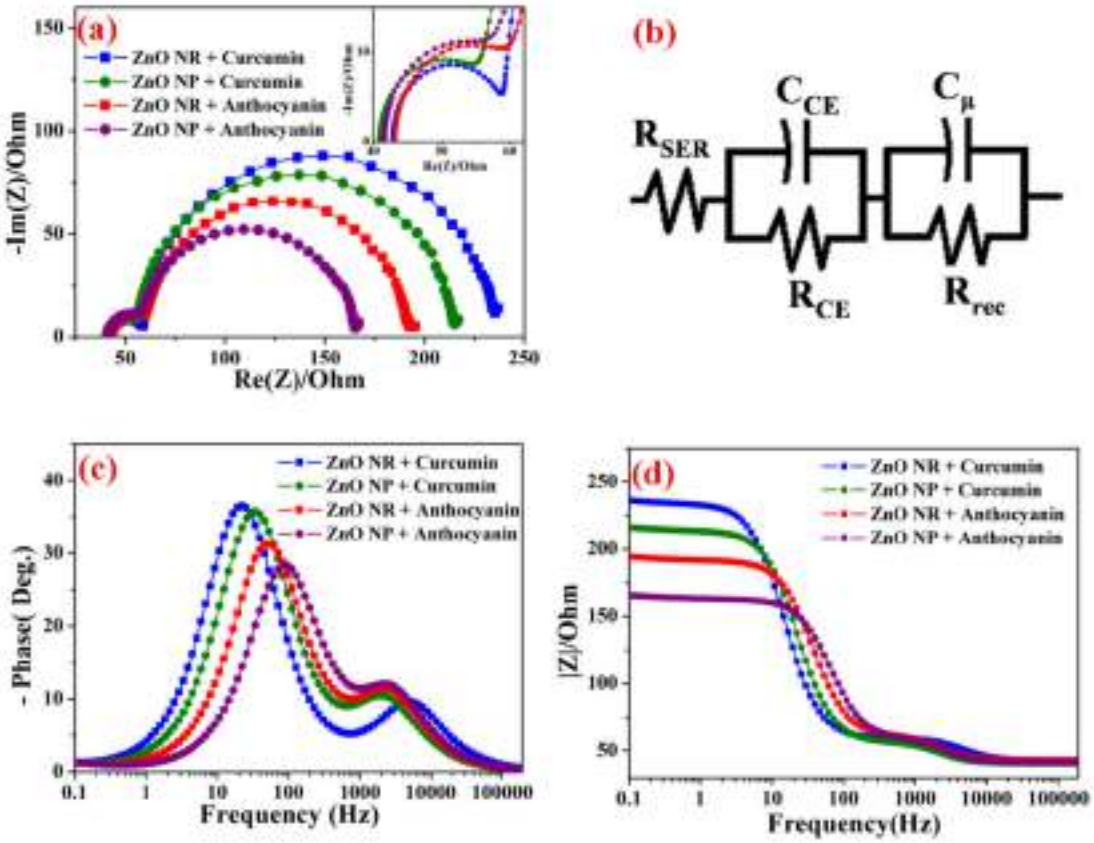

Figure 3.18 EIS spectra of DSSCs (a) Nyquist Plot (b) Equivalent circuit for fitting (c) Bode Phase plot and (d) Bode magnitude plot for impedance.

Table 3.3. Summary of EIS parameters of the DSSCs determined by fitting the experimental data.

Cell Name	Dye used & ZnO microstructure	R_{SER} (Ω)	R_{rec}(Ω)	R_{CE} (Ω)	C_{μ} (μF)	Peak freq. (Hz)	Electron lifetime (τ_e) (ms)
Cell-1	Curcumin & ZnO NR	42.85	173.21	16.28	83.16	22	7.24
Cell-2	Anthocyanin & ZnO NR	40.93	156.37	15.17	59.41	33.29	4.78
Cell-3	Curcumin & ZnO NP	43.25	129.74	17.56	42.52	51	3.12
Cell-4	Anthocyanin & ZnO NP	41.63	103.56	16.85	29.40	88.48	1.80

As all the cells' counter electrodes were prepared using the same procedure, the values of R_{CE} are almost the same for all four cells. Another important representation of the EIS data is Phase and Magnitude bode plots representing Phase (-θ) vs. Frequency (f) and Magnitude of Impedance (|Z|) vs. Frequency curve. Unlike the Nyquist plot, the very important aspect of this plot is that frequency information is not lost. The average carrier lifetime can be estimated from phase bode plots (shown in EIS Fig. 3.18(b)) using the formula

$$\tau_e = \frac{1}{2\pi f_{max}} \qquad (2)$$

where f_{max} represents peak frequency in the mid-frequency range [42]. ZnO NR loaded with Curcumin dye shows the lowest characteristic peak frequency attributing to the highest electron lifetime in the LUMO of the Curcumin dye molecule. It shifts towards higher frequency values for the other cells, which results in decreased electron lifetime(refer to table 3.3).The lowest value of τ_e in ZnO NP cell loaded with anthocyanin (cell-4) extracted from pomegranate juice attributes to the fastest electron recombination leading to degraded overall cell performance.

On the other hand, bode magnitude plots depicted in Fig. 3.18(d) represents the variation of magnitude of impedance with frequency. It may be noted from bode magnitude plot shown in Fig. 3.18.(d) that at low frequencies the magnitude of impedance is high, which indicates higher recombination resistance. But with increase in frequency the impedance starts falling which is due to the faster electron recombination at higher frequencies. In the lower frequency region, the ZnO NR cell sensitized with Curcumin is showing highest magnitude of impedance implying slowest recombination rate, giving rise to highest short circuit current (I_{SC}). In contrary, ZnO NP cell sensitized with anthocyanin extracted from pomegranate fruit shows the lowest impedance in the low frequency region implying fastest recombination process which is reflected in Table 3.3. The possible reason behind these behaviours may be the better adsorption of Curcumin dye molecules over the hexagonal rod shaped ZnO nanostructures in comparison to the other cells. It also can be seen that the value of characteristic frequency shifts towards lower side for increasing value of either R_{rec} or C_{μ}. One more thing can be noted from the impedance plots that the maximum value of phase angle is also decreases with the decrease in value of R_{rec}.

3.4. Conclusions

In this study, hexagonal-shaped ZnO nanorods with preferential growth along (002) plane were successfully grown on ITO substrates using low-cost sol-gel hydrothermal technique. The nanorods have diameters ranging from 100-200nm. XRD study revealed remarkably high crystalline quality of the nanorods. These ZnO nanorod-based substrates were used as photoanodes to prepare DSSCs using natural dyes extracted from pomegranate and turmeric. On the other hand, commercial ZnO nanopowder is also used to fabricate DSSCs using the same natural dyes. Photoelectrochemical performances of all four cells were recorded. From the J-V measurements, a clear enhanced overall cell performance was noticed for the cell constructed using ZnO nanorods and

sensitized using Curcumin dye compared to the other three cells. The probable reason behind this could be the higher amount of Curcumin dye molecule adsorption by the ZnO film due to the better interaction between the carbonyl and hydroxyl groups of Curcumin molecule and the ZnO nanorod film than that of Pomegranate extract. For a deeper understanding of the performances obtained from the cells, the different interfacial mechanisms of the cells were investigated using the EIS technique. It is found that the shape of ZnO nanostructures and different dye molecules present in the extracts affected the electrochemical parameters of the cells. The Best performance of the cell prepared with ZnO nanorod with Curcumin dye is found to be due to highest chemical capacitance (C_μ) along with lowest electron recombination rate and fast charge transport along the ZnO nanorod. Therefore, the Curcumin dye should be an alternative to anthocyanin source for natural dye sensitized solar cells. These results also show that the performances of the natural extract based DSSCs can be enhanced significantly by combining suitable natural dye with the appropriate shape of semiconductor nanostructures and they can become a potential alternative to the synthetic sensitizers based DSSCs. In fact, such combination may results in environment-friendly, remarkably low cost and easily manufacturable dye sensitized solar cells. We can also observe that ZnO based cells are more efficient than TiO_2 based cells when sensitized with Rose Bengal dye.

References:

[1] A. Horvath and E. Rachlew, Nuclear power in the 21st century: Challenges and possibilities, *Ambio* 45 Suppl 1, S38, Jan, (2016).

[2] S. Chu and A. Majumdar, Opportunities and challenges for a sustainable energy future, *nature* 488, 294, (2012).

[3] N. L. Chang, Y. Ho-Baillie, A. Wing, P. A. Basore, T. L. Young, R. Evans and R. J. Egan, A manufacturing cost estimation method with uncertainty analysis and its application to perovskite on glass photovoltaic modules, *Progress in Photovoltaics: Research and Applications* 25, 390, (2017).

[4] A. Kumar, M. Bieri, T. Reindl and A. G. Aberle, Economic Viability Analysis of Silicon Solar Cell Manufacturing: Al-BSF versus PERC, *Energy Procedia* 130, 43, (2017).

[5] M. Grätzel, Dye-sensitized solar cells, *Journal of Photochemistry and Photobiology C: Photochemistry Reviews* 4, 145, (2003).

[6] B. O'regan and M. Grätzel, A low-cost, high-efficiency solar cell based on dye-sensitized colloidal TiO2 films, *nature* 353, 737, (1991).

[7] Y.-T. Kim, J. Park, S. Kim, D. W. Park and J. Choi, Fabrication of hierarchical ZnO nanostructures for dye-sensitized solar cells, *Electrochimica Acta* 78, 417, (2012).

[8] C. Jiang, X. Sun, G. Lo, D. Kwong and J. Wang, Improved dye-sensitized solar cells with a ZnO-nanoflower photoanode, *Applied Physics Letters* 90, 263501, (2007).

[9] J. B. Baxter and E. S. Aydil, Nanowire-based dye-sensitized solar cells, *Applied Physics Letters* 86, 053114, (2005).

[10] A. Jena, S. P. Mohanty, P. Kumar, J. Naduvath, V. Gondane, P. Lekha, J. Das, H. K. Narula, S. Mallick and P. Bhargava, Dye sensitized solar cells: a review, *Transactions of the Indian Ceramic Society* 71, 1, (2012).

[11] J. Gong, J. Liang and K. Sumathy, Review on dye-sensitized solar cells (DSSCs): fundamental concepts and novel materials, *Renewable and Sustainable Energy Reviews* 16, 5848, (2012).

[12] S. Hao, J. Wu, Y. Huang and J. Lin, Natural dyes as photosensitizers for dye-sensitized solar cell, *Solar energy* 80, 209, (2006).

[13] H. Zhu, H. Zeng, V. Subramanian, C. Masarapu, K.-H. Hung and B. Wei, Anthocyanin-sensitized solar cells using carbon nanotube films as counter electrodes, *Nanotechnology* 19, 465204, (2008).

[14] Y. Amao and T. Komori, Bio-photovoltaic conversion device using chlorine-e6 derived from chlorophyll from Spirulina adsorbed on a nanocrystalline TiO2 film electrode, *Biosensors and Bioelectronics* 19, 843, (2004).

[15] K.-H. Park, T.-Y. Kim, S. Han, H.-S. Ko, S.-H. Lee, Y.-M. Song, J.-H. Kim and J.-W. Lee, Light harvesting over a wide range of wavelength using natural dyes of gardenia and cochineal for dye-sensitized solar cells, *Spectrochimica Acta Part A: Molecular and Biomolecular Spectroscopy* 128, 868, (2014).

[16] F. Shao, J. Sun, L. Gao, S. Yang and J. Luo, Growth of various TiO2 nanostructures for dye-sensitized solar cells, *The Journal of Physical Chemistry C* 115, 1819, (2010).

[17] X. Mao, R. Zhou, S. Zhang, L. Ding, L. Wan, S. Qin, Z. Chen, J. Xu and S. Miao, High efficiency dye-sensitized solar cells constructed with composites of TiO 2 and the hot-bubbling synthesized ultra-small SnO 2 nanocrystals, *Scientific reports* 6, 19390, (2016).

[18] D. Maheswari and D. Sreenivasan, Review of TiO2 nanowires in dye sensitized solar cell, *Applied Solar Energy* 51, 112, (2015).

[19] B. Roose, S. Pathak and U. Steiner, Doping of TiO 2 for sensitized solar cells, *Chemical Society Reviews* 44, 8326, (2015).

[20] M. S. Ahmad, A. Pandey and N. A. Rahim, Advancements in the development of TiO2 photoanodes and its fabrication methods for dye

sensitized solar cell (DSSC) applications. A review, *Renewable and Sustainable Energy Reviews* 77, 89, (2017).

[21] K. Tennakone, G. Kumara, A. Kumarasinghe, P. Sirimanne and K. Wijayantha, Efficient photosensitization of nanocrystalline TiO2 films by tannins and related phenolic substances, *Journal of Photochemistry and Photobiology A: Chemistry* 94, 217, (1996).

[22] J. A. Anta, E. Guillen and R. Tena-Zaera, ZnO-based dye-sensitized solar cells, *The Journal of Physical Chemistry C* 116, 11413, (2012).

[23] Ü. Özgür, Y. I. Alivov, C. Liu, A. Teke, M. Reshchikov, S. Doğan, V. Avrutin, S.-J. Cho and H. Morkoc, A comprehensive review of ZnO materials and devices, *Journal of applied physics* 98, 11, (2005).

[24] H. Bae, M. Yoon, J. Kim and S. Im, Photodetecting properties of ZnO-based thin-film transistors, *Applied Physics Letters* 83, 5313, (2003).

[25] Q. Zhang, C. S. Dandeneau, X. Zhou and G. Cao, ZnO nanostructures for dye-sensitized solar cells, *Advanced Materials* 21, 4087, (2009).

[26] Y. Zhang, M. K. Ram, E. K. Stefanakos and D. Y. Goswami, Synthesis, characterization, and applications of ZnO nanowires, *Journal of Nanomaterials* 2012, 20, (2012).

[27] T. Senthil, N. Muthukumarasamy and M. Kang, ZnO nanorods based dye sensitized solar cells sensitized using natural dyes extracted from beetroot, rose and strawberry, *Bulletin of the Korean Chemical Society* 35, 1050, (2014).

[28] S.-i. Kawano, Y. Inohana, Y. Hashi and J.-M. Lin, Analysis of keto-enol tautomers of curcumin by liquid chromatography/mass spectrometry, *Chinese Chemical Letters* 24, 685, (2013).

[29] M. Viuda-Martos, J. Fernández-López and J. Pérez-Álvarez, Pomegranate and its many functional components as related to human health: a review, *Comprehensive Reviews in Food Science and Food Safety* 9, 635, (2010).

[30] B. Pradhan, S. K. Batabyal and A. J. Pal, Vertically aligned ZnO nanowire arrays in Rose Bengal-based dye-sensitized solar cells, *Solar Energy Materials and Solar Cells* 91, 769, (2007).

[31] F. Zhang, C. a. Di, N. Berdunov, Y. Hu, Y. Hu, X. Gao, Q. Meng, H. Sirringhaus and D. Zhu, Ultrathin Film Organic Transistors: Precise Control of Semiconductor Thickness via Spin-Coating, *Advanced Materials* 25, 1401, (2013).

[32] A. H. Kurda, Y. M. Hassan and N. M. Ahmed, Controlling diameter, length and characterization of zno nanorods by simple hydrothermal method for solar cells, *World Journal of Nano Science and Engineering* 5, 34, (2015).

[33] H. Zhou, L. Wu, Y. Gao and T. Ma, Dye-sensitized solar cells using 20 natural dyes as sensitizers, *Journal of Photochemistry and Photobiology A: Chemistry* 219, 188, (2011).

[34] M. Murayama and T. Mori, Equivalent circuit analysis of dye-sensitized solar cell by using one-diode model: effect of carboxylic acid treatment of TiO2 electrode, *Japanese journal of applied physics* 45, 542, (2006).

[35] M. Wang, A. M. Anghel, B. Marsan, N.-L. Cevey Ha, N. Pootrakulchote, S. M. Zakeeruddin and M. Grätzel, CoS supersedes Pt as efficient electrocatalyst for triiodide reduction in dye-sensitized solar cells, *Journal of the American Chemical Society* 131, 15976, (2009).

[36] L. Tao, Z. Huo, Y. Ding, Y. Li, S. Dai, L. Wang, J. Zhu, X. Pan, B. Zhang and J. Yao, High-efficiency and stable quasi-solid-state dye-sensitized solar cell based on low molecular mass organogelator electrolyte, *Journal of Materials Chemistry A* 3, 2344, (2015).

[37] S. S. Negi, Integrated Electronic, Optical, and Structural Features in Pseudo-3D Mesoporous TiO2–X Delivering Enhanced Dye-Sensitized Solar Cell Performance, *ACS Omega* 3, 1645, (2018).

[38] G. Di Carlo, A. Orbelli Biroli, M. Pizzotti, F. Tessore, V. Trifiletti, R. Ruffo, A. Abbotto, A. Amat, F. De Angelis and P. R. Mussini, Tetraaryl

ZnII Porphyrinates Substituted at β-Pyrrolic Positions as Sensitizers in Dye-Sensitized Solar Cells: A Comparison with meso-Disubstituted Push–Pull ZnII Porphyrinates, *Chemistry-A European Journal* 19, 10723, (2013).

[39] J. Bisquert, Chemical capacitance of nanostructured semiconductors: its origin and significance for nanocomposite solar cells, *Physical Chemistry Chemical Physics* 5, 5360, (2003).

[40] F. Fabregat-Santiago, E. M. Barea, J. Bisquert, G. K. Mor, K. Shankar and C. A. Grimes, High carrier density and capacitance in TiO2 nanotube arrays induced by electrochemical doping, *Journal of the American Chemical Society* 130, 11312, (2008).

[41] J. Akilavasan, K. Wijeratne, H. Moutinho, M. Al-Jassim, A. Alamoud, R. Rajapakse and J. Bandara, Hydrothermally synthesized titania nanotubes as a promising electron transport medium in dye sensitized solar cells exhibiting a record efficiency of 7.6% for 1-D based devices, *Journal of Materials Chemistry A* 1, 5377, (2013).

[42] P. Bhatt, K. Pandey, P. Yadav, B. Tripathi and M. Kumar, Impedance spectroscopic investigation of the degraded dye-sensitized solar cell due to ageing, *International Journal of Photoenergy*, (2016). DOI: 10.1155/2016/8523150